Growth Engineering of CH3NH3PbI3 Structures for High-Efficiency Solar Cells

ARTICLE *in* ADVANCED ENERGY MATERIALS · NOVEMBER 2015

Impact Factor: 16.15 · DOI: 10.1002/aenm.201501358

5 AUTHORS, INCLUDING:

Mojtaba Abdi Jalebi

University of Cambridge

11 PUBLICATIONS **54** CITATIONS

SEE PROFILE

Md Khaja Nazeeruddin

École Polytechnique Fédérale de Lausanne

484 PUBLICATIONS **43,102** CITATIONS

SEE PROFILE

Growth Engineering of $CH_3NH_3PbI_3$ Structures for High-Efficiency Solar Cells

M. Ibrahim Dar, Mojtaba Abdi-Jalebi, Neha Arora, Michael Grätzel, and Mohammad Khaja Nazeeruddin**

Controlling the growth of perovskite crystals has been one of the interesting strategies to mold their fundamental properties and exploit their potential in the fabrication of high performance solar cells. Herein, the impact of chloride on the conversion of lead halide into $CH_3NH_3PbI_3$, morphology, and coverage of perovskite structures using modified two-step approach is investigated systematically, which eventually dictates the overall performance of the resulting device. Structural and morphological characterization is thoroughly carried out by X-ray diffraction and field emission scanning electron microscopy, respectively. Various spectroscopic techniques provide ample evidence that $CH_3NH_3PbI_3$ structures formed in the presence of chloride, in the lead halide precursor solution, exhibit desired properties, such as fewer defects. Moreover, the morphology of $CH_3NH_3PbI_3$ structures and surface coverage of the resulting layers are considerably different from those obtained in the absence of chloride. After gaining a rational understanding regarding the effect of chloride on the growth, morphology, and optical properties of $CH_3NH_3PbI_3$ structures, fabrication of devices revealing a power conversion efficiency of over 16% under standard AM 1.5 G illumination is realized. The fundamental understanding and high efficiency reported here distinguishes our results, particularly where chloride based precursors are involved.

1. Introduction

Increasing demands for the fabrication of low-cost, highly efficient light harnessing devices have compelled the photovoltaic community to investigate newer materials that have eventually led to the evolution of mixed organic–inorganic perovskite solar cells.[1] Exploration of organic–inorganic lead halide perovskites, i.e., $CH_3NH_3PbX_3$ (X = Br, I) as light-harnessing materials in photoelectrochemical cells was initiated by Kojima et al. by documenting a power conversion efficiency of 3.8% for $CH_3NH_3PbI_3$.[2] Later, organic–inorganic lead halide perovskites received immediate attention from photovoltaic community, as these light-absorbing materials, exhibit enticing optical, excitonic, and electrical properties that are suitable for the development of low-cost high-efficiency solar cells.[3–7]

Of the various properties exhibited by the mixed organic–inorganic metal halide perovskites, the spontaneous dissociation of excitons and efficient charge extraction are the most desired ones.[8] These properties are subservient to the formation and nature of the perovskites which allows their tuning by controlling the growth of perovskite materials.[9] In tailoring the morphology and coverage of perovskite layer, low-cost solution-based bottom-up approaches have been more facile as compared to other methods used for the preparation of perovskite material.[10] In the literature, various synthetic approaches have been documented explaining how to achieve a precise control over the growth and morphology of perovskites.[11] Specifically, changing the chemical environment during the formation of perovskites has been found as a potential tool to control their morphology.[12] Although chloride has been widely explored as a growth controlling and directing agent, studies pertaining to unravel the role and confirm the presence of chloride in $CH_3NH_3PbI_3$ are debatable. Recently, we have reported that under given conditions, the chloride ions influence the growth of the $CH_3NH_3PbI_3$ and careful studies based on STEM energy dispersive spectroscopy (EDS) study indicated that the $CH_3NH_3PbI_3$ perovskites formed are chloride-free.[12]

Enhancement of short-circuit current in solution-processed planar $CH_3NH_3PbI_3$ solar cells was reported by Docampo et al.[13] after adding an appropriate amount of chloride in the methyl ammonium iodide solution. Nevertheless, using EDS and electron energy loss spectroscopy, authors could not detect any signal corresponding to chloride. Yu et al.[14] studied perovskite films which were prepared from $CH_3NH_3I/PbCl_2$ and CH_3NH_3I/PbI_2 precursor combinations and demonstrated that the function of chloride is to allow the removal of excess

Dr. M. I. Dar, Dr. N. Arora, Prof. M. K. Nazeeruddin
Group for Molecular Engineering of Functional Materials
Institute of Chemical Sciences and Engineering
École Polytechnique Fédérale de Lausanne
CH-1015-Lausanne, Switzerland
E-mail: ibrahim.dar@epfl.ch; mdkhaja.nazzeruddin@epfl.ch
M. Abdi-Jalebi
Cavendish Laboratory
Department of Physics
University of Cambridge
JJ Thomson Avenue
Cambridge CB3 0HE, UK
Dr. M. I. Dar, Prof. M. Grätzel
Laboratory of Photonics and Interfaces
Institute of Chemical Sciences and Engineering
École Polytechnique Fédérale de Lausanne
CH-1015 Lausanne, Switzerland

DOI: 10.1002/aenm.201501358

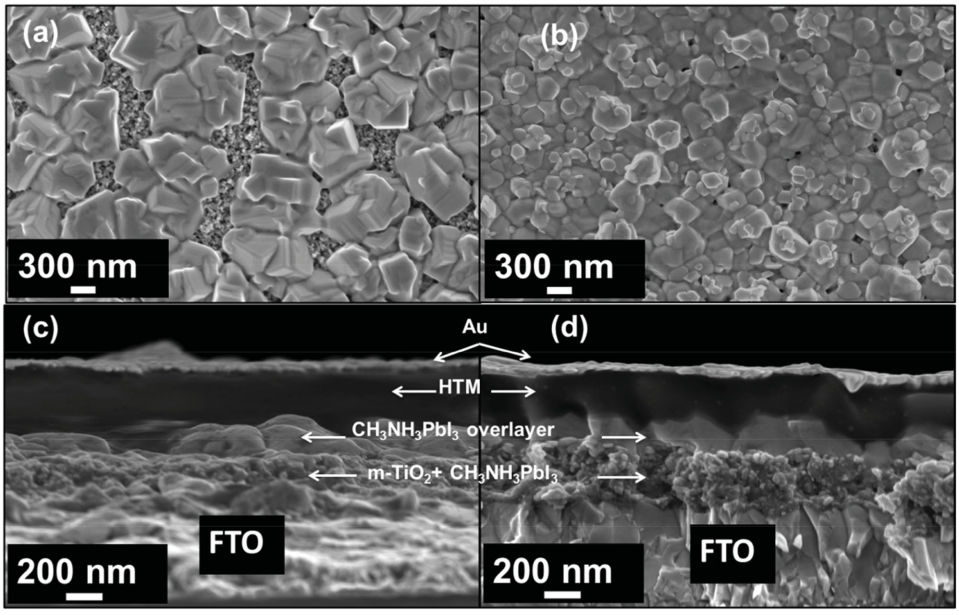

Figure 1. Scanning electron microscopy analysis of perovskite structures. Top view of a) pure $CH_3NH_3PbI_3$ structures supported on mesoporous TiO_2 photoanode, b) $CH_3NH_3PbI_3$ structures supported on a mesoporous TiO_2 scaffold obtained after using PbI_2 precursor solution containing 2% $PbCl_2$. SEM cross-sectional images of complete devices based on c) reference, and d) $CH_3NH_3PbI_3$ obtained after using 2% $PbCl_2$.

$CH_3NH_3^+$ and the role of latter ($CH_3NH_3^+$) is to slow down the perovskite formation process. Moreover, the authors were able to detect a negligible amount of Cl content in annealed perovskite films by employing depth-profile X-ray photoelectron spectroscopy. In a similar direction, Williams et al.[15] carried out comprehensive studies and elucidated the structure directing role played by the chloride in the formation of $CH_3NH_3PbI_3$ films. Furthermore, not merely experimental observations even theoretical calculations showed that the preferential position of chloride is at the TiO_2 interface as compared to bulk perovskite.[16]

Herein, we explored the impact of chloride ions on the morphology and coverage of $CH_3NH_3PbI_3$ layer using modified sequential deposition approach.[5] Steady state photoluminescence (PL) techniques showed simply that the $CH_3NH_3PbI_3$ structures formed in the presence of chloride exhibit less defects. Structural characterization using X-ray diffraction (XRD) was used to study the extent of lead halide conversion into perovskite, while as morphological characterization based on field emission scanning electron microscopy (FESEM) brought out that shape and coverage of the $CH_3NH_3PbI_3$ structures prepared in the presence of chloride is considerably different from a chloride-free reference. After gaining a rational understanding regarding the effect of the chloride on the growth, conversion, and morphology of perovskite structures, fabrication of devices revealing a reproducible power conversion efficiency (PCE) of over 16% was realized. Such a high efficiency together with fundamental insights distinguishes our work particularly where chloride-based precursors are involved. Overall, such a comprehensive study will further contribute toward the fundamental understanding of the impact of chloride on the properties and performance of the perovskite solar cells.

2. Results and Discussion

The impact of chloride on the conversion of lead iodide into $CH_3NH_3PbI_3$ and the overall performance of the resulting perovskite device was contemplated. To deposit perovskite onto ≈250 nm thick TiO_2 photoanode films, a modified sequential deposition approach was used (for details see Experimental section). Typically, after spin-coating $(PbI_2)_{1-x}(PbCl_2)_x$ ($x = 0.02$–0.1), the synthesis of different perovskite samples was realized by spin coating isopropyl alcohol solution containing methylamonium iodide (MAI) under optimized conditions. Due to the poor solubility of $PbCl_2$ in *N,N*-dimethylformamide (DMF), dimethylsulfoxide (DMSO) was chosen as a preferred solvent. Tidhar et al. reported that due to its limited solubility, small $PbCl_2$ nanoparticles are present in the DMF precursor solutions, which could act as heterogeneous nucleation sites for the perovskite crystal formation.[17]

2.1. Morphological Characterization

The surface morphology of the $CH_3NH_3PbI_3$ deposited on mesoporous TiO_2 photoanode was examined by FESEM. **Figure 1**a,b displays the SEM top view of reference and $CH_3NH_3PbI_3$ film obtained in the presence of 2% $PbCl_2$. High magnification SEM (Figure 1a) revealed that the reference $CH_3NH_3PbI_3$ film is composed of relatively larger asymmetric structures which only cover partially the underlying mesoscopic TiO_2 scaffold. By contrast, $CH_3NH_3PbI_3$ films (Figure 1b) obtained in the presence of 2% $PbCl_2$ are densely packed forming a contiguous film that covers the entire nanocrystalline TiO_2 layer. The formation of densely packed perovskite structures ostensibly improved the surface coverage of films obtained in the presence of 2% $PbCl_2$.

To evaluate the impact of $PbCl_2$ further, we increased its concentration to 5% and 10%. However, under similar conditions no appreciable improvement in coverage was observed (Figure S1, Supporting Information). Therefore, from SEM analysis we contend that the composition of precursor solution, such as the presence of small amounts of $PbCl_2$ in PbI_2 or a mixture of both lead halides, can lead to the formation of $CH_3NH_3PbI_3$ structures exhibiting entirely different dimensions, morphology, and coverage over the mesoporous TiO_2 films. This is in accordance with the previous studies in which it was observed that $PbCl_2$ in two-step methodology improves the surface coverage of $CH_3NH_3PbI_3$ film without chloride occupying its lattice.[12,15]

2.1.1. Cross-Sectional SEM

After spin coating spiro-OMeTAD as the hole-transporting material (HTM) on $CH_3NH_3PbI_3$ layer, the device was completed by thermal evaporation of 70 nm gold layer as the back contact. The cross-sectional SEM image acquired from the reference device (Figure 1c) reveals an inhomogeneous $CH_3NH_3PbI_3$ overlayer which is covered with a less uniform layer of HTM. By contrast, cross-sectional SEM analysis of the device in which $CH_3NH_3PbI_3$ film was obtained in the presence of 2% $PbCl_2$ (Figure 1d) displays that 100 nm thick $CH_3NH_3PbI_3$ overlayer is uniformly covered by the HTM, i.e., spiro-OMeTAD, atop the 260 nm thick TiO_2 photoanode. Such an observation based on cross-sectional SEM is in agreement with the top view SEM image (Figure 1a,b) showing the surface coverage of $CH_3NH_3PbI_3$ overlayer. Arguably, the improved coverage could avoid the formation of parasitic contact such as, HTM/TiO_2, which is detrimental to the performance of the devices.

2.2. Structural Characterization

To ascertain the conversion of PbI_2 into $CH_3NH_3PbI_3$ in the presence of $PbCl_2$, structural characterization of the resulting perovskite films was carried out using XRD. All the peaks indexable to the tetragonal structure of $CH_3NH_3PbI_3$ could be found in the XRD patterns (**Figure 2**).[18] Although XRD showed well crystallinity of the resulting perovskite films, however while using more than 2% $PbCl_2$ in the precursor solution, a feature at $2\theta = \approx 12.6°$ appeared which could be indexed to unconverted PbI_2. With the increase in the concentration of $PbCl_2$, the intensity of the unconverted PbI_2 peak ≈12.6° increases which arguably confirms the slower rate of conversion of PbI_2 into $CH_3NH_3PbI_3$. Within the detection limit of XRD, no peak shift was observed in the XRD patterns of reference and other samples. However, the ratio of peak intensities of (220)/(310) planes was found to pronounce by increasing the amount of $PbCl_2$ up to 5% in the lead halide precursor solution which possibly explains the role of the chloride ions in orienting the growth of $CH_3NH_3PbI_3$ structures. Earlier, it has been reported that the Cl induces a preferred orientation in $CH_3NH_3PbI_3$ crystalline grains.[19] Surprisingly, by increasing the concentration of $PbCl_2$ further to 10%, the intensity of (310) planes enhanced relatively

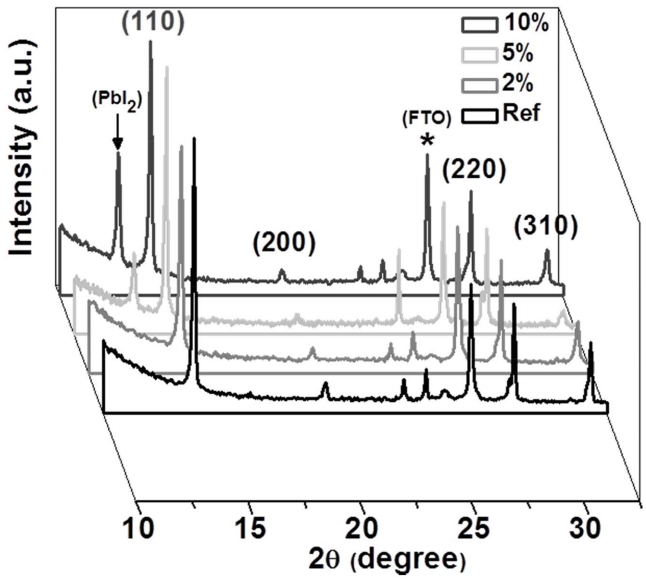

Figure 2. X-ray diffraction patterns of perovskite samples. XRD patterns of $CH_3NH_3PbI_3$ supported on TiO_2 photoanode obtained after using different concentration of $PbCl_2$.

which could explain that in orienting the crystal growth of $CH_3NH_3PbI_3$, a critical amount of $PbCl_2$ is required.

2.3. Spectroscopic Studies

2.3.1. UV–Vis Absorption

Figure 3a shows the UV–vis absorption spectra of $CH_3NH_3PbI_3$ samples. The general features of the absorption spectra are in a good agreement with the reports documented in the literature.[20] All the perovskite films exhibit two absorption peaks at 480 nm and 780 nm corresponding to the excitation of electrons from two valence bands to the conduction band.[21] The understanding of the high energy transition band (≈480 nm) is still unclear as it has also been attributed to charge transfer.[22]

Substituting iodide of $CH_3NH_3PbI_3$ with chloride, i.e., formation of $CH_3NH_3PbI_{3-x}Cl_x$ is expected to increase the band gap of the perovskite material and a blueshift in the band edge absorption (780 nm) would confirm the chloride doping of $CH_3NH_3PbI_3$. However, the absence of observable shift in ≈780 nm absorption band indicates that $CH_3NH_3PbI_3$ are chloride-free.[23] It is well established that due to the lattice mismatch, $CH_3NH_3PbI_3$ and $CH_3NH_3PbCl_3$ do not form solid solutions.[23]

2.3.2. Photoluminescence Study

To evaluate the impact of changing the chemical ambiance on the optical properties during the formation of $CH_3NH_3PbI_3$, we recorded steady state PL upon exciting the samples at 460 nm. As shown in Figure 3a, the general features of the PL spectra are in accordance with those of room temperature PL spectra reported in the literature.[24] Although we did not observe any

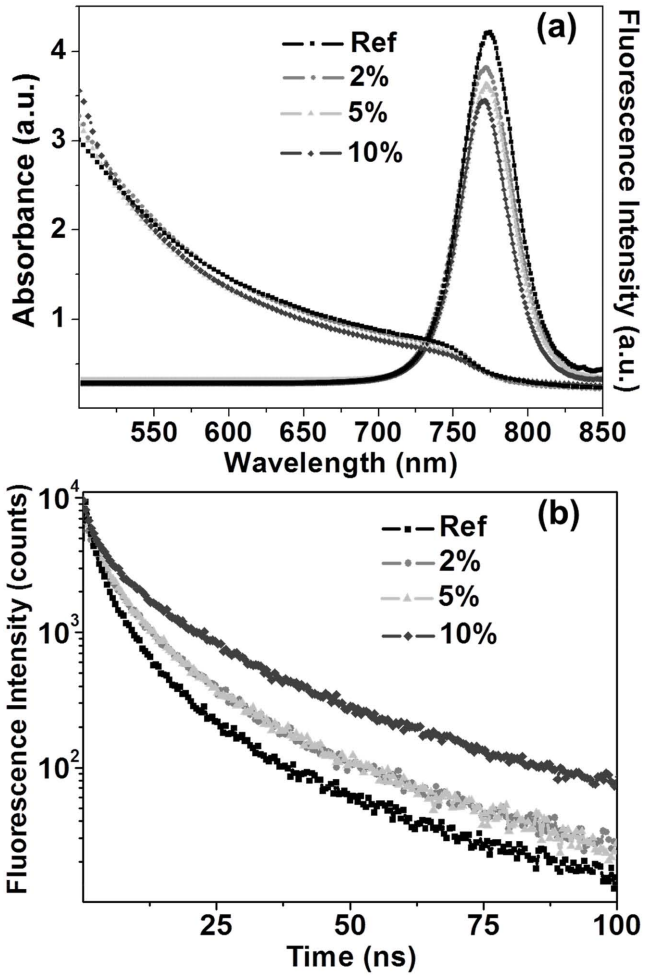

Figure 3. Spectroscopic studies of perovskite samples obtained after varying the concentration of $PbCl_2$. a) Steady state absorption and fluorescence spectra and b) fluorescence decay kinetics measured at 780 nm upon excitation at 406 nm of reference and perovskite films obtained after using different concentration of $PbCl_2$.

significant shift in the PL peak at 775 nm, a mild asymmetric shift observed in the longer wavelength region of emission feature was witnessed that has been attributed to the passivation of traps or defects present at various interfaces or within $CH_3NH_3PbI_3$ materials.[25] It is worth mentioning that the absence of shift in the PL peak demonstrate that the presence of chloride does not influence the band gap or dimensions of the $CH_3NH_3PbI_3$ structures.[26]

2.3.3. Life Time Measurements

Improvement in the surface coverage and passivation of defects, as evident from SEM and steady state emission studies, respectively, could influence the dynamics of critical process such as electron–hole recombination. Therefore, we carried out fluorescence lifetime measurements using time-correlated single photon counting technique. Fluorescence decay kinetics of various perovskite films deposited on mesoporous TiO_2 is shown in Figure 3b. Depending on the concentration of $PbCl_2$ used for the growth of $CH_3NH_3PbI_3$ films, fluorescence decay kinetics brought out variations both in the fast as well as slow components of the decay curve.[27] From the decay curve, it is quite evident that the recombination is the fastest in the reference $CH_3NH_3PbI_3$ sample (Figure 3b, black trace) and by increasing the concentration of $PbCl_2$ recombination decreased monotonically, possibly due to the formation of well-connected $CH_3NH_3PbI_3$ structures exhibiting less concentration of traps, as confirmed by steady state PL.

2.4. Photovoltaic Performance

Devices obtained under different conditions, as summarized in Table S1 in the Supporting Information, were analyzed under AM 1.5G solar irradiation. **Figure 4**a shows the *J–V* characteristics of the best performing devices based on the structure: Fluorine doped tin oxide (FTO)/compact TiO_2/mesoporous TiO_2/$CH_3NH_3PbI_3$/HTM/Au (Figure 1c,d). Under illumination intensity of 100 mW cm^{-2}, the reference device exhibits a short-circuit current density (J_{SC}) of 20.5 mA cm^{-2}, an open-circuit voltage (V_{OC}) of 986 mV and a fill factor (FF) of 0.71, resulting in an overall PCE (η) of 14.3%. Overall, the best performance was revealed by a device obtained while using 2% $PbCl_2$ which exhibits a J_{SC} of 21.1 mA cm^{-2}, a V_{OC} of 1053 mV, and a FF of 0.73, resulting in the overall PCE (η) of 16.2%. From **Table 1**, it is evident that the presence of chloride mainly improved the V_{OC} from 986 mV (reference device) to 1053 mV (while using 2% $PbCl_2$). Recently Xu et al. reported a two-step solution deposition method by spin coating a mixture solution of CH_3NH_3Cl (MACl) and CH_3NH_3I onto the TiO_2/PbI_2 film. It was found that the inclusion of MACl improves the crystallinity and surface coverage of perovskite which in turn leads to an enhancement in the *Voc* owing to the reduction of reverse saturation current density.[28] In our case, both the trend and high PCE was quite reproducible. Such a high performance could be due to the confluence of complete conversion of PbI_2 with the uniform coverage of $CH_3NH_3PbI_3$ overlayer and less traps, as established by structural, morphological, and spectroscopic studies.

Although the coverage of $CH_3NH_3PbI_3$ overlayer (Figure S1, Supporting Information) remains the same by increasing the concentration of $PbCl_2$ to 10%, the systematic diminution in the performance of devices, mostly because of low V_{oc} and fill factor was observed (Table 1) which could be attributed to the incomplete conversion of lead halide to $CH_3NH_3PbI_3$ under given conditions. The PCE (Table S2, Supporting Information) exhibits quite reproducible enhancement from 14% to 16%, after mixing 2% $PbCl_2$ with PbI_2 which contrasts with the report in which the highest PCE of 14% was obtained while using 10% $PbCl_2$.[29] Arguably this disagreement could arise from adopting different experimental conditions and synthetic methodology. The modified two-step approach employed here led to the preparation and deposition of perovskite films which are relatively much smoother and are composed of well-connected perovskite structures. Furthermore, use of DMSO instead of DMF as a solvent for $PbCl_2$ is found to be very crucial for obtaining high PCE which could be attributed to the higher solubility of $PbCl_2$ in DMSO.

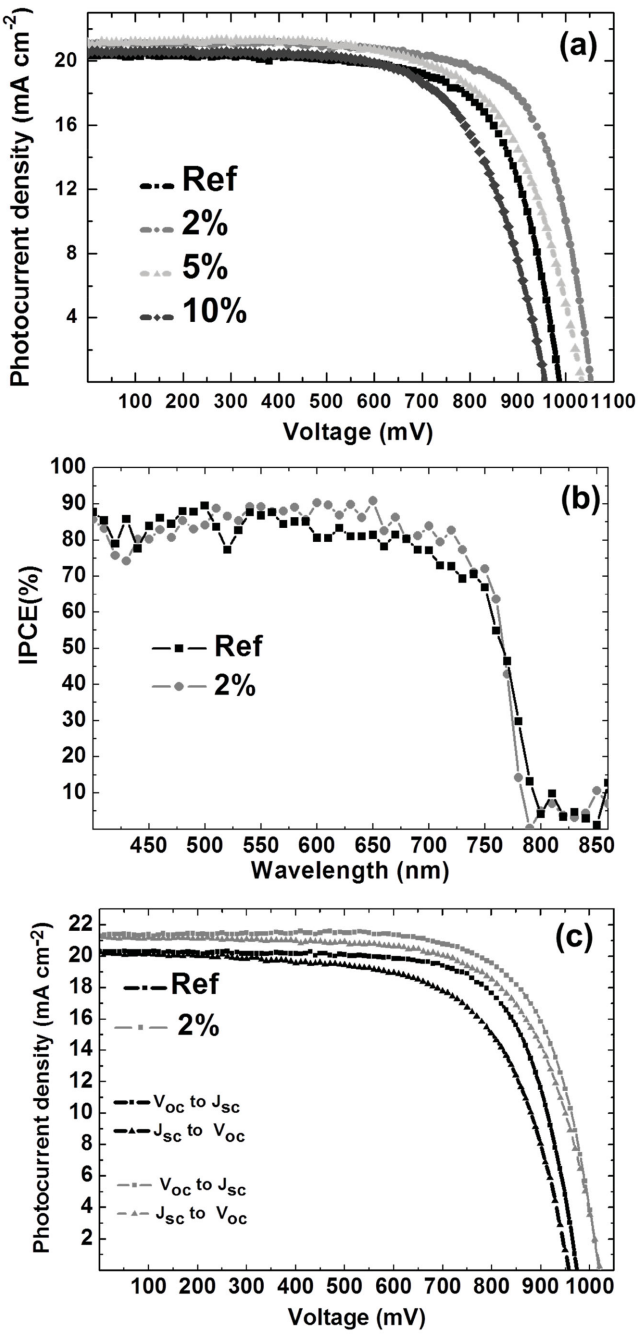

Figure 4. Photovoltaic studies of perovskite devices obtained with varying concentration of $PbCl_2$. a) Current–voltage characteristics of devices recorded at a scan rate of 0.1 V s^{-1} under illumination of 100 mW cm^{-2}, b) IPCE spectra as a function of the wavelength of monochromatic light for the reference and the device obtained after using 2% $PbCl_2$, and c) Current–voltage hysteresis recorded for the reference and the device obtained after using 2% $PbCl_2$ at a scan rate of 0.1 V s^{-1} under stimulated AM1.5 100 mW cm^{-2} photon flux.

Seok and co-workers prepared $CH(NH_2)_2PbI_3$ films using intramolecular exchange approach and achieved a maximum PCE of over 20% from the devices based on them.[30] The intramolecular exchange process involves formation of $CH(NH_2)_2PbI_3$ by direct exchange of DMSO molecules

Table 1. Summary of the photovoltaic parameters derived from *J–V* measurements for the different devices (showing the best performance) fabricated using modified sequential deposition method.

$(PbI_2)_{1-x}(PbCl_2)_x$	J_{SC} [mA cm^{-2}]	V_{OC} [mV]	FF [%]	η [%]
$x = 0$	20.5	986	71	14.3
$x = 0.02$	21.1	1053	73	16.2
$x = 0.05$	21.1	1034	67	14.6
$x = 0.10$	20.6	957	67	13.2

intercalated in PbI_2 with $CH(NH_2)_2$ cations. Recently, Park and co-workers reported fabrication of highly reproducible perovskite solar cells via Lewis base adduct of PbI_2.[31] A 1:1:1 adduct of MAI:PbI_2:DMSO was obtained from DMF solution containing equimolar MAI, PbI_2, and DMSO. An average PCE of 18.3% and best PCE of 19.7% was achieved by exploiting the adduct chemistry. Li et al. employed a series of $PbI_2(DMSO)_x$ ($0 \le x \le 1.86$) complexes obtained via solution process.[32] After systematic optimization, the $PbI_2(DMSO)_{1.22}$ complex lead to the fabricating of perovskite solar cell with a PCE of 17.2%.

The aforementioned literature employed a higher concentration of DMSO solvent whereas in our work the best performance was achieved using a $((PbI_2\text{-}DMF)_{98}:(PbCl_2\text{-}DMSO)_{02})$ mixture, in which the concentration of DMSO is comparatively negligible. Nevertheless, given the involvement of DMSO in the evolution of highly efficient perovskite solar cells, the role of DMSO present even in trace amounts cannot be underestimated.

2.4.1. Incident Photon-to-Current Efficiency

Furthermore, external quantum efficiency or incident photon-to-current efficiency (IPCE) (Figure 4b) of the reference and the best photovoltaic device as a function of wavelength shows that the generation of photocurrent begins at ≈780 nm, which is in accordance with the band gap of pure $CH_3NH_3PbI_3$.[33] The response of the best performing photovoltaic device to light reveals a IPCE of ≈85% and the photocurrents obtained from the IPCE data are in good agreement with those of current–voltage (*J–V*) measurements. In addition to other favorable factors, such as complete conversion of PbI_2 into $CH_3NH_3PbI_3$, higher IPCE specifically in the higher wavelength region could be due to the formation of smoother films in case of devices obtained after using 2% $PbCl_2$.[34]

2.4.2. Hysteresis

Scan speed dependent hysteresis observed in the photocurrent–voltage curves of perovskite solar cells could be a bottleneck in the development of photovoltaic technology based on them.[35] Various studies regarding the origin of hysteresis have been documented but the fundamental understanding of it still remains inconclusive.[36] Toward this end, Shao et al. reported that the presence of charge trap states on the surface and grain boundaries of the perovskite materials as the origin of the hysteresis and were also able to eliminate it by

Table 2. Summary of the experimental conditions used for the synthesis of different perovskite structures and photovoltaic performance of the devices based on them.

Device	Precursors used	J_{SC} [mA cm^{-2}]	V_{OC} [mV]	FF [%]	η [%]
S1	1.2 M PbI_2 and MAI* (8 mg mL^{-1})	19.0	919	71	12.6
S2	1.2 M $PbCl_2$ and MAI (8 mg mL^{-1})	15.2	894	62	8.6
S3	1.2 M PbI_2, MAI:MACl* (95:5) wt% in (8 mg mL^{-1})	8.8	688	52	3.2

*(MAI and MACl are the acronyms for methyl ammonium iodide and methyl ammonium chloride, respectively).

passivizing these trap states.[25] Tress et al. attributed the hysteresis to the build-up of space charge close to the contacts due to the ionic displacement within the $CH_3NH_3PbI_3$ perovskite solar cells.[37] Recently Eames et al. identified vacancy assisted migration of iodide ions with an activation energy of 0.6 eV and suggested that organic–inorganic lead halide perovskites are mixed ionic–electronic conductors.[38] In our case, from the comparative analysis of hysteresis curves recorded for the reference and the device obtained after using 2% $PbCl_2$ (Figure 4c), we conclude that morphology and coverage of $CH_3NH_3PbI_3$ overlayer play a great role in influencing the hysteresis in the photocurrent–voltage curves. Wojciechowski et al. showed that by modifying the TiO_2 interface with C_{60}, a decrease in hysteretic behavior was observed which was attributed to the enhanced electron transfer.[39] In this study, the combination of favorable factors, such as uniform coverage and crystal formation brings down the concentration of charge traps present on the surfaces and interfaces or within $CH_3NH_3PbI_3$. Moreover, a diminution in the hysteresis of devices obtained after using 2% $PbCl_2$ could be attributed to the passivation of traps that was evident from a mild asymmetric shift in the lower energy side of the emission peak.

It is well known that the photovoltaic performance of a device is strongly influenced by the experimental conditions employed for the preparation of $CH_3NH_3PbI_3$.[40–42] So far, we have demonstrated the influence of chloride on the growth and performance of the perovskite solar cells using the modified conversion method. We also changed the source of chloride, from $PbCl_2$ to CH_3NH_3Cl and the methodology from a modified two-step to a conventional two-step approach for the deposition of perovskite (**Table 2**). We fabricated two different types of devices which were based on the organic–inorganic halide perovskite materials and were grown in the ambiance of chloride ions using the sequential method. Previously, we have studied such organic–inorganic halide perovskite structures using STEM-EDS which revealed clearly that the resulting $CH_3NH_3PbI_3$ materials are chloride-free.[12] For a comparative analysis, we fabricated a device in which $CH_3NH_3PbI_3$ prepared by adopting sequential deposition method in chloride-free condition, was used as the light harnessing material.

The morphology obtained by SEM of the three different samples is shown in **Figure 5**. The SEM image of S1 displays the aerial view of rough perovskite overlayer composed of polydisperse crystals (Figure 5a). On the contrary, SEM analysis

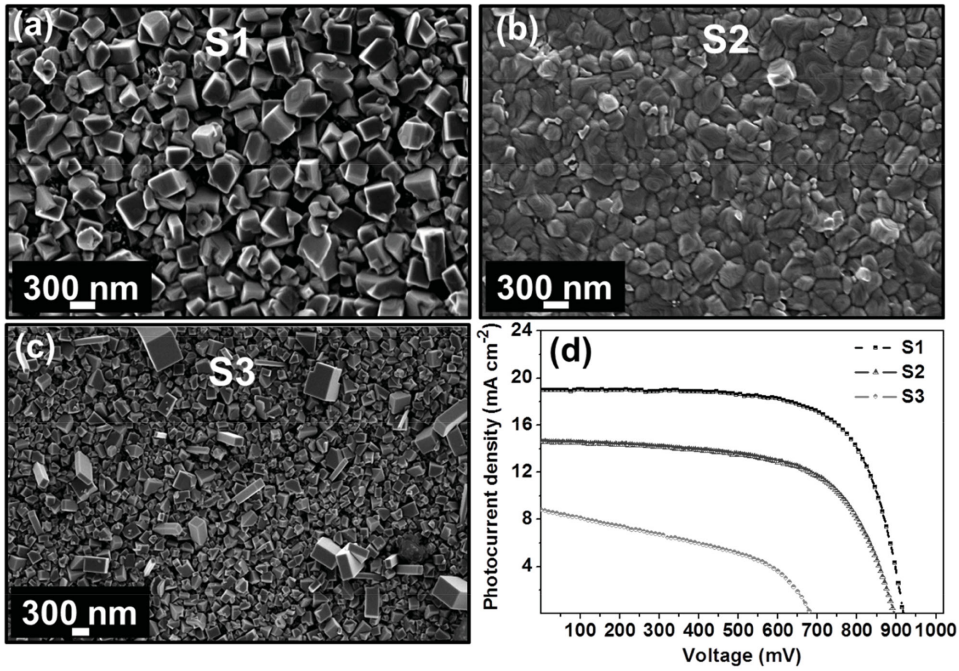

Figure 5. Perovskite structures grown in the ambiance of different halide sources. SEM analysis: Top view of a) pure $CH_3NH_3PbI_3$ structures, b) $CH_3NH_3PbI_3$ obtained after using pure $PbCl_2$, c) $CH_3NH_3PbI_3$ obtained after using 5 mol% CH_3NH_3Cl (all samples are supported on mesoporous TiO_2 photoanode), and d) Current–voltage characteristics of devices under the illumination of 98 mW cm^{-2}.

of sample S2 (Figure 5b) brought out the formation of relatively smoother perovskite overlayer while as similar studies on S3 sample (Figure 5c) established the presence of elongated perovskite structures.

Devices based on S1, S2, and S3 films (as summarized in Table 2) were analyzed under solar irradiation (Figure 5d). Under illumination of 98 mW cm^{-2}, the device S1 exhibits a short-circuit current density (J_{SC}) of 19 mA cm^{-2}, an open-circuit voltage (V_{OC}) of 919 mV and a fill factor (FF) of 0.71, resulting in an overall conversion efficiency (η) of 12.6%. From the comparative analysis, devices (S1) based on pure iodide precursors were found to provide the best overall performance. In addition to a lower $J_{SC,}$ S2 and S3 showed lower V_{OC}, which probably could be attributed to the incomplete conversion of $PbCl_2$[12] and to the recombination at perovskite/gold interface (elongated perovskite nanorods in contact with Au back contact), respectively. Although the surface analysis based on SEM revealed that the perovskite overlayer in case of S2 sample is relatively smooth, however the device based on it displayed poor performance. From this observation and without any contextualization, we contend that formation of smoother perovskite films alone is not a sufficient condition to achieve high PCE.

3. Conclusion

Contemplation regarding the impact of chloride on the growth, properties, and performance of $CH_3NH_3PbI_3$ solar cells has been carried out. A small amount of chloride not only oriented the growth and improved the surface coverage of $CH_3NH_3PbI_3$ overlayer, but also facilitated the formation of perovskite material exhibiting fewer defects which was established by structural, morphological, and spectroscopic studies, respectively. The confluence of these favorable factors led to the enhancement of PCE to above 16%. Furthermore, as compared to reference device, the most efficient devices that were obtained in the presence of 2% chloride, revealed a minimal hysteresis. Observation of such a low hysteresis could be attributed to the presence of fewer defects. Previously, we have documented that "defects define a device" and observed that the presence of spectator ions could influence the defect concentration within the nanostructures.[43] We envisage that the passivation of traps present at the various interfaces or the formation of perovskite material exhibiting fewer number of traps could bring down the anomalous hysteresis in the perovskite solar cells. We also contend that the modification of sequential technique by introducing a small amount of lead chloride in the PbI_2 precursor provides a judicious control over the growth of $CH_3NH_3PbI_3$ structures. Finally, the detailed studies presented herewith will further contribute toward the fundamental understanding of the perovskite based-solar cells.

4. Experimental Section

Photoanode Preparation and Device Fabrication: The FTO (NSG 10, Nippon sheet glass, Japan) substrate was cleaned with a detergent, rinsed with water and ethanol, and then treated with a UV/O_3 cleaner for 15 min. TiO_2 compact layer was deposited on the substrates by aerosol spray pyrolysis at 450 °C using a commercial titanium diisopropoxide bis(acetylacetonate) solution (75% in 2-propanol, Sigma-Aldrich) diluted in ethanol (Sigma-Aldrich) (1:9, volume ratio) as precursor and oxygen as carrier gas. The TiO_2 commercial paste (Dyesol 30NRD) was spin coated onto a precleaned FTO glass containing spray deposited ≈40 nm thick TiO_2 compact layer. After going through a series of sintering steps (325 °C for 5 min with 15 min ramp time, 375 °C for 5 min with 5 min ramp time, 450 °C for 15 min with 5 min ramp time, and 500 °C for 15 min with 5 min ramp time), the sintered TiO_2 films were used as a photoanode.

Deposition of $CH_3NH_3PbI_3$ using Modified Sequential Method: 1.2 M solutions of PbI_2 (99%, Aldrich) and $PbCl_2$ (Sigma Aldrich) were prepared, respectively, in DMF (Sigma Aldrich) and DMSO (Sigma Aldrich) solvent by constant stirring at 80 °C for 30 min. Due to the limited solubility of $PbCl_2$ in DMF, DMSO was chosen as a preferred solvent. The TiO_2 photoanode films were then coated with PbI_2 containing 0, 2, 5, and 10 mol% of $PbCl_2$ by spin coating at 6500 rpm for 30 s, and dried at 80 °C for 15 min. Lead halide precursor solution containing x mol% of $PbCl_2$ into PbI_2 was obtained by mixing volumes in the ratio of x:100–x. To achieve higher loading of PbI_2, the deposition was repeated twice. After cooling to room temperature, a solution (200 µL) of CH_3NH_3I in 2-propanol (8 mg mL^{-1}) was spin coated on the resulting PbI_2 films with a delay of 120 s for 30 s, and were dried at 80 °C for 30 min. Spin-coating of CH_3NH_3I solution is a very critical step and it should be carried out by flushing 200 µL in a single flow, after resting the tip at one of the corners of the substrate.

Deposition of Perovskites Using Sequential Method: Deposition of PbI_2 or $PbCl_2$ onto TiO_2 photoanode films was carried out as mentioned above. Instead of spin coating MAI solution, the films were dipped in a solution of CH_3NH_3I in 2-propanol (8 mg mL^{-1}) for 4 and 2 min at room temperature in case of S1 and S2, respectively, or in a mixture of CH_3NH_3I:CH_3NH_3Cl (95:5) wt% in 2-propanol (8 mg mL^{-1}) for 4 min at 60 °C (in case of S3), rinsed with 2-propanol for 2 s. All the films were annealed at 80 °C for 30 min.

Deposition of Spiro-OMeTAD: The spiro-OMeTAD was deposited by spin-coating (4000 rpm, 30 s) 40 µL of solution prepared by dissolving 72.3 mg (2,2′,7,7′-tetrakis (*N*,*N*-di-*p*-methoxyphenylamine)-9,9-spirobifluorene) (spiro-OMeTAD), 17.5 µL of a stock solution of 520 mg mL^{-1} bis(trifluoromethylsulphonyl)imide in acetonitrile, and 29 µL of a stock solution of 300 mg mL^{-1} tris(2-(1H-pyrazol-1-yl)-4-*tert*-butylpyridine)cobalt(III) bis(trifluoromethylsulphonyl)imide in acetonitrile, and 28.8 µL 4-*tert*-butylpyridine in 1 mL chlorobenzene. The device fabrication was carried out under controlled atmospheric conditions with humidity <1% and was finally completed by thermally evaporating 70 nm of gold layer as back contact.

Materials Characterization: A field-emission scanning electron microscope (FESEM, Merlin) was employed to analyze the morphology of the samples. An electron beam accelerated to 3 kV was used with an in-lens detector. XRD data were collected on a Bruker Advance D8 X-ray diffractometer with a graphite monochromator, using Cu Kα radiation, at a scanning rate of 0.5 deg min^{-1}.

Optical Characterization: The steady state optical properties of perovskite films were studied using UV–Vis absorption and fluorescence spectroscopy. The absorption spectra of perovskite films were recorded with convenient UV–Vis–NIR spectrophotometer (CARY-5) in transmission mode. Fluorescence spectra and fluorescence decay kinetics were recorded on a spectrofluorometer Fluorolog 322. Fluorescence spectra were recorded by exciting the samples from the FTO side with 450 W Xenon lamp at a fixed wavelength of 460 nm and scanning the emission monochromator from 500 to 850 nm. Same spectrometer working in a single-photon counting mode was used for the measurements of fluorescence decay kinetics with subnanosecond time resolution. Picosecond pulsed diode laser head NanoLED-405LH (Horiba) emitting <200 ps duration pulses at 406 nm with repetition rate of 1 MHz and pulse energy about 11 pJ was used as an excitation source.

Photovoltaic Characterization: A 450 W xenon lamp (Oriel, USA) was used as the light source for photovoltaic (*J*–*V*) measurements. The spectral output of the lamp was filtered using a Schott K113 Tempax sunlight filter (Präzisions Glas & Optik GmbH, Germany) to reduce the

mismatch between the simulated and actual solar spectrum to less than 2%. The *J–V* characteristics of the devices were recorded with a Keithley model 2400 digital source meter (Keithley, USA). The photoactive area of 0.16 cm^2 was defined using a dark-colored metal mask. Incident IPCE measurements were made using a 300 W xenon light source (ILC Technology, USA). A double-monochromator spectrometer (Gemini-180, Jobin Yvon Ltd. UK) was used to select and increment the wavelength of the radiation impinging on the cells. The monochromatic incident light was passed through a chopper running at 1 Hz and the on/off ratio was measured by an operational amplifier. This was superimposed on a white light bias corresponding to an intensity of 10 mW cm^{-2}.

Supporting Information

Supporting Information is available from the Wiley Online Library or from the author.

Acknowledgements

The authors acknowledge the European Community's Seventh Framework Programme (FP7/2007–2013) under Grant Agreement No. 281063 of the Powerweave project for financial support. N.A. gratefully acknowledges financial support from the Swiss confederation under Swiss Government Scholarship programme. The authors acknowledge funding from the European Union Seventh Framework Programme [FP7/2007–2013] under Grant Agreement No. 604032 of the MESO project, (FP7/2007–2013) ENERGY.2012.10.2.1; NANOMATCELL, Grant Agreement No. 308997. M.I.D. and M.G. thank the King Abdulaziz City for Science and Technology (KACST) for financial support. The authors acknowledge financial support by Swiss National Science Foundation (SNF) through SNF-NRP70(407040-154056/1).

Received: July 7, 2015
Revised: September 29, 2015
Published online:

[1] P. Gao, M. Gratzel, M. K. Nazeeruddin, *Energy Environ. Sci.* **2014**, *7*, 2448.
[2] A. Kojima, K. Teshima, Y. Shirai, T. Miyasaka, *J. Am. Chem. Soc.* **2009**, *131*, 6050.
[3] G. C. Papavassiliou, *Mol. Cryst. Liq. Cryst.* **1996**, *286*, 231.
[4] M. M. Lee, J. Teuscher, T. Miyasaka, T. N. Murakami, H. J. Snaith, *Science* **2012**, *338*, 643.
[5] J. Burschka, N. Pellet, S.-J. Moon, R. Humphry-Baker, P. Gao, M. K. Nazeeruddin, M. Gratzel, *Nature* **2013**, *499*, 316.
[6] K. Tanaka, T. Takahashi, T. Ban, T. Kondo, K. Uchida, N. Miura, *Solid State Commun.* **2003**, *127*, 619.
[7] A. Mei, X. Li, L. Liu, Z. Ku, T. Liu, Y. Rong, M. Xu, M. Hu, J. Chen, Y. Yang, M. Grätzel, H. Han, *Science* **2014**, *345*, 295.
[8] S. D. Stranks, G. E. Eperon, G. Grancini, C. Menelaou, M. J. P. Alcocer, T. Leijtens, L. M. Herz, A. Petrozza, H. J. Snaith, *Science* **2013**, *342*, 341.
[9] D. Shi, V. Adinolfi, R. Comin, M. Yuan, E. Alarousu, A. Buin, Y. Chen, S. Hoogland, A. Rothenberger, K. Katsiev, Y. Losovyj, X. Zhang, P. A. Dowben, O. F. Mohammed, E. H. Sargent, O. M. Bakr, *Science* **2015**, *347*, 519.
[10] J.-H. Im, I.-H. Jang, N. Pellet, M. Grätzel, N.-G. Park, *Nat. Nanotechnol.* **2014**, *9*, 927.
[11] N. J. Jeon, J. H. Noh, Y. C. Kim, W. S. Yang, S. Ryu, S. I. Seok, *Nat. Mater.* **2014**, *13*, 897.
[12] M. I. Dar, N. Arora, P. Gao, S. Ahmad, M. Grätzel, M. K. Nazeeruddin, *Nano Lett.* **2014**, *14*, 6991.
[13] P. Docampo, F. C. Hanusch, S. D. Stranks, M. Döblinger, J. M. Feckl, M. Ehrensperger, N. K. Minar, M. B. Johnston, H. J. Snaith, T. Bein, *Adv. Energy Mater.* **2014**, *4*, 1400355.
[14] H. Yu, F. Wang, F. Xie, W. Li, J. Chen, N. Zhao, *Adv. Funct. Mater.* **2014**, *24*, 7102.
[15] S. T. Williams, F. Zuo, C.-C. Chueh, C.-Y. Liao, P.-W. Liang, A. K. Y. Jen, *ACS Nano* **2014**, *8*, 10640.
[16] S. Colella, E. Mosconi, G. Pellegrino, A. Alberti, V. L. P. Guerra, S. Masi, A. Listorti, A. Rizzo, G. G. Condorelli, F. De Angelis, G. Gigli, *J. Phys. Chem. Lett.* **2014**, *5*, 3532.
[17] Y. Tidhar, E. Edri, H. Weissman, D. Zohar, G. Hodes, D. Cahen, B. Rybtchinski, S. Kirmayer, *J. Am. Chem. Soc.* **2014**, *136*, 13249.
[18] K. Liang, D. B. Mitzi, M. T. Prikas, *Chem. Mater.* **1998**, *10*, 403.
[19] G. Grancini, S. Marras, M. Prato, C. Giannini, C. Quarti, F. De Angelis, M. De Bastiani, G. E. Eperon, H. J. Snaith, L. Manna, A. Petrozza, *J. Phys. Chem. Lett.* **2014**, *5*, 3836.
[20] S. De Wolf, J. Holovsky, S.-J. Moon, P. Löper, B. Niesen, M. Ledinsky, F.-J. Haug, J.-H. Yum, C. Ballif, *J. Phys. Chem. Lett.* **2014**, *5*, 1035.
[21] G. Xing, N. Mathews, S. Sun, S. S. Lim, Y. M. Lam, M. Grätzel, S. Mhaisalkar, T. C. Sum, *Science* **2013**, *342*, 344.
[22] K. G. Stamplecoskie, J. S. Manser, P. V. Kamat, *Energy Environ. Sci.* **2015**, *8*, 208.
[23] N. Pellet, J. Teuscher, J. Maier, M. Grätzel, *Chem. Mater.* **2015**, *27*, 2181.
[24] C. Wehrenfennig, M. Liu, H. J. Snaith, M. B. Johnston, L. M. Herz, *J. Phys. Chem. Lett.* **2014**, *5*, 1300.
[25] Y. Shao, Z. Xiao, C. Bi, Y. Yuan, J. Huang, *Nat. Commun.* **2014**, *5*, 5784.
[26] V. D'Innocenzo, A. R. Srimath Kandada, M. De Bastiani, M. Gandini, A. Petrozza, *J. Am. Chem. Soc.* **2014**, *136*, 17730.
[27] a) S. D. Stranks, V. M. Burlakov, T. Leijtens, J. M. Ball, A. Goriely, H. J. Snaith, *Phys. Rev. Appl.* **2014**, *2*, 034007; b) M. I. Dar, M. Abdi-Jalebi, N. Arora, T. Moehl, M. Grätzel, M. K. Nazeeruddin, *Adv. Mater.* **2015**, *27*, 7221.
[28] Y. Xu, L. Zhu, J. Shi, S. Lv, X. Xu, J. Xiao, J. Dong, H. Wu, Y. Luo, D. Li, *ACS Appl. Mater. Interfaces* **2015**, *7*, 2242.
[29] S. Dharani, H. A. Dewi, R. R. Prabhakar, T. Baikie, C. Shi, D. Yonghua, N. Mathews, P. P. Boix, S. G. Mhaisalkar, *Nanoscale* **2014**, *6*, 13854.
[30] W. S. Yang, J. H. Noh, N. J. Jeon, Y. C. Kim, S. Ryu, J. Seo, S. I. Seok, *Science* **2015**, *348*, 1234.
[31] N. Ahn, D.-Y. Son, I.-H. Jang, S. M. Kang, M. Choi, N.-G. Park, *J. Am. Chem. Soc.* **2015**, *137*, 8696.
[32] W. Li, J. Fan, J. Li, Y. Mai, L. Wang, *J. Am. Chem. Soc.* **2015**, *137*, 10399.
[33] M. I. Dar, F. J. Ramos, Z. Xue, B. Liu, S. Ahmad, S. A. Shivashankar, M. K. Nazeeruddin, M. Grätzel, *Chem. Mater.* **2014**, *26*, 4675.
[34] N. Marinova, W. Tress, R. Humphry-Baker, M. I. Dar, V. Bojinov, S. M. Zakeeruddin, M. K. Nazeeruddin, M. Grätzel, *ACS Nano* **2015**, *9*, 4200.
[35] H. J. Snaith, A. Abate, J. M. Ball, G. E. Eperon, T. Leijtens, N. K. Noel, S. D. Stranks, J. T.-W. Wang, K. Wojciechowski, W. Zhang, *J. Phys. Chem. Lett.* **2014**, *5*, 1511.
[36] R. S. Sanchez, V. Gonzalez-Pedro, J.-W. Lee, N.-G. Park, Y. S. Kang, I. Mora-Sero, J. Bisquert, *J. Phys. Chem. Lett.* **2014**, *5*, 2357.
[37] W. Tress, N. Marinova, T. Moehl, S. M. Zakeeruddin, M. K. Nazeeruddin, M. Gratzel, *Energy Environ. Sci.* **2015**, *8*, 995.
[38] C. Eames, J. M. Frost, P. R. F. Barnes, B. C. O'Regan, A. Walsh, M. S. Islam, *Nat. Commun.* **2015**, *6*, 7497.
[39] K. Wojciechowski, S. D. Stranks, A. Abate, G. Sadoughi, A. Sadhanala, N. Kopidakis, G. Rumbles, C.-Z. Li, R. H. Friend, A. K. Y. Jen, H. J. Snaith, *ACS Nano* **2014**, *8*, 12701.
[40] N. J. Jeon, J. H. Noh, W. S. Yang, Y. C. Kim, S. Ryu, J. Seo, S. I. Seok, *Nature* **2015**, *517*, 476.
[41] F. Hao, C. C. Stoumpos, D. H. Cao, R. P. H. Chang, M. G. Kanatzidis, *Nat. Photonics* **2014**, *8*, 489.
[42] J.-H. Im, H.-S. Kim, N.-G. Park, *APL Mater.* **2014**, *2*, 081510.
[43] M. Ibrahim Dar, N. Arora, N. Pratap Singh, S. Sampath, S. A. Shivashankar, *New J. Chem.* **2014**, *38*, 4783.